Title

THE PROMPT GAMMA RAY, PROMPT ELECTRON AND PROMPT X-RAY SPECTRA ASSOCIATED WITH FISSION FRAGMENTS OF SPECIFIC MASS

Authors

Bowman, Harry R.
Thompson, Stanley G.
Watson, Rand L.
et al.

Publication Date

1965-01-27

UCRL-11902

University of California

Ernest O. Lawrence Radiation Laboratory

THE PROMPT GAMMA RAY, PROMPT ELECTRON AND PROMPT X-RAY SPECTRA ASSOCIATED WITH FISSION FRAGMENTS OF SPECIFIC MASS

Berkeley, California

DISCLAIMER

Submitted for presentation in the I. A. E. A. Symposium on the Physics and Chemistry of Fission, Salzburg, Austria, March 22—26, 1965.

UCRL-11902

UNIVERSITY OF CALIFORNIA

Lawrence Radiation Laboratory
Berkeley, California

AEC Contract No. W-7405-eng-48

THE PROMPT GAMMA RAY, PROMPT ELECTRON AND PROMPT X-RAY SPECTRA ASSOCIATED WITH FISSION FRAGMENTS OF SPECIFIC MASS

Harry R. Bowman, Stanley G. Thompson, Rand L. Watson, S. S. Kapoor and John O. Rasmussen

January 27, 1965

THE PROMPT GAMMA RAY, PROMPT ELECTRON AND PROMPT X-RAY SPECTRA ASSOCIATED WITH FISSION FRAGMENTS OF SPECIFIC MASS

Harry R. Bowman, Stanley G. Thompson, Rand L. Watson, S. S. Kapoor* and John O. Rasmussen

Lawrence Radiation Laboratory
University of California
Berkeley, California

January 27, 1965

ABSTRACT

Well defined prompt gamma-rays, prompt-conversion electrons and prompt K X-rays have been observed in coincidence with moving fission fragments of Cf^{252}. In a few cases, the masses and charges of the nuclei emitting the gamma rays and conversion electrons have been identified.

The gamma-ray, prompt-electron and prompt X-ray energies as well as the two fission fragments' energies were measured with high-resolution solid-state detectors. The masses of the fragments were deduced from their energies, and the nuclear charges were determined by measuring the K X-ray energies associated with different masses. The magnitude and sign of the Doppler shift in gamma-ray energy allowed assignment of the gamma-ray lines to single members of fragment pairs. The Doppler shift also provides an independent measure of the fragment velocity and hence the fragment mass after neutron emission.

The results of the X-ray measurements are consistent with the view that the majority of the prompt X-rays emitted during the spontaneous fission of Cf^{252} is the result of internal conversion during the de-excitation of low energy collective states of the primary fission fragments.

Apart from the specific results discussed above, we feel that the most important consequence of our experiments has been the demonstration that it is possible to study the properties of individual fission fragments, as identified

by their characteristic radiations (rather than studying the properties of an average fission fragment with an average mass and charge). The consequences of this advance in the technique of studying fission fragments are being explored.

1. Introduction

It is the purpose of this paper to present results obtained from a detailed experimental study of the prompt gamma rays, prompt electrons and prompt X-rays emitted in the spontaneous fission of Cf^{252}, in particular, from the investigations of the energy distributions of these radiations as a function of the mass of the fission fragments.

The aim of such an extensive study is to provide a body of experimental data from which a number of general features of the fission process may be deduced, and against which proposed theories may be tested. The study of these prompt radiations, in addition, provides a potential means of investigating the final stages in the de-excitation mechanism of very neutron rich nuclei. We would like to stress that our principal objective here is to present experimental results in a reasonably complete manner, and that a theoretical interpretation has not been aimed at.

This work is a continuation of a more general study [1-3] covering all of the prompt radiations associated with spontaneous fission, which has been in progress at this laboratory over the years since the discovery of Cf^{252} [4].

In the first series of experiments, the energies of the prompt gamma rays in coincidence with the fission fragments were measured with a NaI gamma-ray detector. The sorting of these spectra with respect to the fragment mass ratios revealed a large number of discrete gamma-ray energies. These measurements were further extended by using a high resolution lithium-drifted germanium gamma-ray detector. The dependence of these gamma-ray energies on the velocity and direction of motion of the fragments showed that many of these gamma rays were emitted from moving fragments. These Doppler shifts in the gamma-ray energies provided an effective means of identifying the emitting fragment of a fragment pair.

The second series of experiments was carried out to measure the electron spectra in coincidence with fission. The sorting of the electron data according to the fragment masses also revealed a number of peaks which were predominately concentrated in the low energy region. The structure in the conversion electron spectra was found to be clearly associated with the previously measured gamma-ray lines.

The third series of experiments involved the measurements of the energies of K X-rays with a lithium-drifted silicon detector in coincidence with fission fragments. The data have been analyzed to obtain the most probable charge (Z_p) of the individual fragments, the number of the X-rays emitted per fragment, and the average time of the X-ray emission from different fragments. A by-product of the X-ray measurements has been the independent

and direct measurement of the nuclear charge of californium.

2. Experimental Apparatus

Figure 1 shows the experimental arrangement used in these experiments. A weightless Cf^{252} fission source, prepared by self-transfer onto a thin nickel foil, was placed between two solid state fission detectors. The first series of experiments was done using a NaI counter for gamma ray detection which was mounted in line with the two fission detectors along the axis of fission (Fig. 1). The high resolution gamma-ray measurements were made by replacing the NaI detector with a lithium-drifted germanium detector operated at liquid nitrogen temperature. In the cases of the electron spectra and the X-ray measurements, a lithium-drifted silicon detector operated at dry ice temperature was used. In each of the experiments, pulses from the three detectors were fed to standard transistor amplifiers and then to a triple coincidence unit of the zero-cross over type having a time resolution of 50 ns. The chance coincidence rate in all of the measurements was less than 1% of the true coincidence rate. If the pulses from the three detectors were in coincidence, then the amplifier outputs were stored in temporary memory #1. The three detector pulse heights were then analyzed serially by the pulse-height analyzer. The digital outputs of the pulse-height analyzer were in turn stored in correlated form in memory #2. The output of memory #2 was written on magnetic tape each time after memory #2 became full. The magnetic tape could be read back at the end of each run, and the data could be observed just as they came in during the experiment.

In order to eliminate electronic drift during the runs, digital stabilizers of the type described by Nakamura and La Pierre [5] were used. For the pulse height stabilization during the gamma-ray work, a Na^{22} source of positron annihilation radiation was placed between the fission gamma-ray detector and a second NaI detector as shown in Fig. 1. Whenever a double coincidence between the two 511 keV gamma radiations was observed, the temporary memory and the pulse-height analyzer were informed that the radiation detected by the fission gamma-ray detector was not a fission fragment gamma ray, but a 511 keV annihilation photon. The digital output of the pulse-height analyzer was then compared to a predetermined channel number to check the gain of the system. If the gain had changed, then a d. c. signal was sent to the appropriate variable gain preamp to stabilize the gain of the system. The pulse-height dispersion introduced by the system was always less than 0.1%. A number of different sources were used for stabilization during the many different experiments, depending on the radiation detected and the energy range involved. The fission fragment

detectors were stabilized in a very similar way.

3. Data Handling

The triple coincidence pulse-height data recorded on magnetic tape for each of these experiments were processed on the IBM 7094 computer. The fission fragment energies were obtained by normalizing the first moments of the light and heavy fragment pulse-height distributions to the first moments of the respective energy distributions obtained previously by time-of-flight measurements [6]. The fission fragment masses were first calculated using momentum conservation and the relation between energy and mass. By use of the relationships between the average number of neutrons as a function of fragment mass and total kinetic energy (obtained from earlier measurements [2,3]), an iterative type of calculation was carried out to obtain the fragment masses before and after neutron emission. The triple coincidence data in each case were sorted on the computer according to the masses of the fragments after neutron emission and in some cases, according to the total kinetic energy of the fragments.

4. Prompt Gamma Rays

When the NaI gamma-ray energy spectra were sorted according to fission fragment mass ratio, a number of definite peaks appeared in the energy range from 150 to 600 keV. The spectra changed markedly for different mass ratios as shown in Fig. 2b, which explains why the discrete structure is nearly obscured in a total prompt gamma-ray spectrum such as that given in Fig. 2a, where no sorting according to mass ratio or direction is made. The spectra shown in Fig. 2b were subject to a further restriction such that only gamma rays emitted from fission events in which heavy fragments were traveling toward the gamma detector were counted. The dependence of the energy of the gamma rays on the direction of motion of the fragments can be seen by comparing the two spectra shown in Fig. 2c. The dashed and solid lines represent the gamma-ray spectra for the two cases: (1) when the heavy fragments ($M = 140 \pm 2$) were moving towards the gamma-ray detector and (2) away from the detector. From the measured sign and the magnitude of the Doppler shift, it is, therefore, possible to identify the emitting fragment of the fragment pair.

Measurements with lithium-drifted germanium gamma-ray detectors have resulted in a great improvement in the gamma-ray energy resolution. Spectra for the energy range of 300 to 600 keV are shown in Fig. 3a and 3b (for the mass intervals 109 to 111 and 137 to 139) for the two cases: (1) light

fragments traveling towards the gamma-ray detector and (2) heavy fragments traveling towards the gamma-ray detector. Individual gamma-ray peaks are well-resolved, and by comparison of Figs. 3a and 3b, the energies can be corrected for Doppler shift and the peaks identified with heavy or light fragments. Inspection of Fig. 3 shows three peaks identified with light fragments (E, I, L) and twelve identified (and labeled alphabetically) with heavy fragments. These lines will be discussed later in the analysis of the electron data.

Figure 4 is a three-dimensional model of the gamma-ray spectra in the energy range below 300 keV for each mass group ranging from 90 to 165. These spectra are more complex than those in the high energy region, and only about a dozen of the lines in Fig. 4 have been assigned to definite fragments.

In Figs. 5a, b, c, and d, the effect of sorting the low energy gamma-ray data according to total kinetic energy for a single mass interval is shown. This means of selection can be used to demonstrate that a particular line cannot be associated with neutron capture (n, γ) in or about the gamma-ray crystal. If these lines were indeed coming from neutron capture, the intensities should decrease with increasing total kinetic energy. In Fig. 5 as can be seen, the reverse of this occurs.

5. Prompt Electron Spectra

The prompt electron energies were measured in coincidence with fission fragments by means of a lithium-drifted silicon electron detector. A large (~5,000 gauss) inhomogeneous magnetic field of the configuration proposed by Malmfors [7] was used to steer the electrons around a block of lead, which shielded the electron detector from the fission fragments and gamma rays. Electrons having a wide range of energies precess in a trochoidal orbit in the fringing field of a large electromagnet. The electron detector was mounted inside a vacuum chamber 90° around the magnet from the fission source. The electron spectra in the energy range 300 to 600 keV are shown in Fig. 6 for the mass intervals 107-111 and 137-141.

The geometry of the system was such that only electrons which were emitted near 90° with respect to the fragment flight path were accepted into the electron spectrometer; however, the finite size of the fragment detector and the rather large acceptance angle of the magnetic field introduced an amount of angular dispersion from the strictly 90° configurations. This effect resulted in a considerable broadening of the electron energy peaks and is the predominant contribution to the experimental resolution.

Figure 7 shows a three-dimensional model of the electron spectra below 300 keV. These low energy electron data have been analyzed along with the low energy gamma-ray data, and about a dozen lines have been found that correspond to both sets of data.

6. X-Ray Experiment

The energy distributions of the K X-rays were measured with a lithium-drifted silicon detector operated at dry ice temperatures to obtain the best energy resolution (FWHM = 3.5 keV). The X-ray detector was mounted close to one of the fragment detectors to obtain a high solid angle for the detection of the X-rays emitted from fragments stopped in the fission detector. Figure 8 shows a three-dimensional plot of the observed X-ray energy distributions as a function of the mass of the fragments moving toward the X-ray detector. Figure 9 shows the energy spectra of the X-rays from mass 140 moving (a) toward and (b) away from the detector.

It can be seen from Fig. 9 that the fraction of the fragment X-rays detected is much larger when that particular fragment is moving towards the X-ray detector. This difference in intensity is largely due to the fact that the X-rays are emitted all along the fragment path. From the observed ratio of intensities of X-rays, it has, therefore, been possible to determine the relative solid angle of detection and the average time of X-ray emission from different fragment masses. Figure 10 shows the average time of emission for K X-rays from different fragment masses as obtained from the above analysis.

The observed number of K X-rays per fission, corrected for detector geometry, X-ray attenuation and detection efficiency, are shown as a function of the final mass (M_f) in Fig. 11.

The most probable charge (Z_p), for each mass interval was obtained in the following way. For each value of Z, the expected K X-ray energy distribution curve was computed by the addition of four Gaussian distributions corresponding to the $K\alpha_1$, $K\alpha_2$, $K\beta_1$ and $K\beta_2$, each having a FWHM corresponding to the observed energy resolution and having average energies and intensity ratios as given by Wapstra et. al. [8]. The calculated distributions were compared with the observed X-ray energy distributions to obtain the most probable values.

The plot of measured Z_p versus initial mass of the fragments, A_i, is shown in Fig. 12. (These data have been corrected for mass dispersion effects.)

7. Discussion of Results

7.1 Prompt Gamma-Ray and Prompt Electron Spectra

The results of a preliminary analysis of the gamma-ray and electron data are given in Table I, where a few of the observed gamma-ray lines are listed by their energies (E_γ), along with tentative assignment of mass, A, and proton number, Z. The masses were arrived at by comparing the gamma-ray peak intensities as a function of mass with various spectra obtained at 0°, 90° and 180° with respect to the direction of motion of the fragments. The errors (±1 mass unit) are estimates based on a study of the mass dispersion, associated with these lines, as a function of total kinetic energy.

The atomic numbers were obtained from the K X-ray measurements. The errors (±1 unit of charge) are estimates based on the overall charge dispersion in the X-ray measurements. The last column in Table I, labeled (K electron located), denotes whether a line could be found in the electron data corresponding to a line in the gamma-ray spectra. Selection of the electron and gamma-ray data according to fragment total kinetic energy as well as mass was used as a means of identifying lines associated with both spectra. An example of how this was carried out can be seen by comparing the electron spectra of Fig. 6 with the gamma-ray spectra for the same mass interval in Fig. 2c. There is a general similarity in the gamma-ray structure, for the energy range of 300 to 600 keV, shown in Fig. 2c, obtained with a NaI detector, and in the electron spectra shown in Fig. 6. The three gamma-ray peaks in Fig. 2c (376, 472 and 583 keV) have been found to be associated with the three broad peaks in the electron spectra. Using the higher resolution gamma-ray data from Fig. 3a and 3b with the peaks labeled alphabetically, we have calculated the expected locations of the associated K and L-conversion lines and have plotted them below the electron spectra as shown in Fig. 6.

The limits on the half lives for gamma-ray emission in Table I were estimated from the measured Doppler shifts in gamma-ray energy. The three measured life times were obtained by varying the length of the flight path of the fragments and observing the Doppler shift. The geometry of the electron detection system was such that electrons emitted after 10^{-9} sec would not have been detected and may account for the few cases where electron lines could not be located. Low yield in conversion electrons could also be the result of E1 type gamma-ray transitions.

It is interesting to note that the measured gamma-ray energies associated with masses greater than 144 seem to suggest the existence of

rotational transitions ($4^+ \rightarrow 2^+$, $2^+ \rightarrow 0^+$) indicating the onset of large stable nuclear deformations at about 88 to 90 neutrons. This onset of deformation is consistent with the results of Coulomb excitation studies of stable nuclei in the region of Nd^{150}. Some yield of Nd^{150} can be expected from fission of Cf^{252} and the measured gamma-ray energies for mass 150 do indeed agree with the known 260 and 132 keV energies [9] of the first two excited states of Nd^{150}.

7.2 Emission of X-Rays

The measured half lives for the K X-ray emission (0.1-0.9 ns) are consistent with the view that most of these X-rays are emitted as a result of the process of internal conversion during the de-excitation of the low energy collective states of the primary fission fragments. If any vacancy in the K-shell were created due to the fission act itself, the time of emission of the subsequent X-rays is expected to be much smaller ($\sim 10^{-14}$ sec).

The observed number of K X-rays per fission from the light and the heavy fragment groups are found to be (0.24 ± 0.02) and (0.32 ± 0.02) respectively. The X-ray yield curve shown in Fig. 11 is the result of a combination of complex effects due to variations of the average gamma-ray yield, energy, conversion coefficient and fluorescent yield and their dependence on fragment mass and charge. The abrupt increase in the X-ray yield for fragment masses greater than 144 is consistent with the expected onset of large nuclear deformation in the vicinity of 88 neutrons and is consistent with the measured gamma-ray energies.

The results of our measurements of Z_p versus the initial mass of the fission fragments are shown plotted in Fig. 12. For purposes of comparison, we also show the results of the predictions of several well-known empirical relationships. Therefore, in the figure we show the values of Z_p versus A_i calculated by Milton [10] for the maximum energy release on the basis of Seeger's mass formula. The two other curves shown in Fig. 12 are calculated on the hypothesis of equal charge displacement (ECD) [11] applied to the instant of scission and unchanged charge distribution (UCD). Though none of the above hypotheses fits the data well, the experimental values are found to be in better agreement with the calculated curve based on equal charge displacement (ECD). Glendenin and Unik [12] have also recently determined Z_p versus mass from the X-ray measurements with NaI(Tl) detector, and also found that hypothesis of ECD fits their data better. A detailed plot of the measured charges in our experiments is shown in Fig. 13, where the deviations of the measured charge from the unchanged specific charge (UCD) are plotted for both the light and the heavy fragments on a complimentary scale. The

fact that the data points corresponding to the light and the heavy fragments describe the same curve indicates that the sum of the measured charges of the complimentary fragments do indeed add up to 98 within the experimental uncertainty of 0.2 units. The sum of the charges of the complimentary fragments, averaged over all the events, was actually found to be (97.9 ± 0.2).

It can be seen from Fig. 13 that, in general, the fragments in the light group have a higher specific charge than those in the heavy group. However, this does not appear to be true within each group itself. The trend of variation of charge density with the fragment mass as observed in the present work is quite similar to that obtained in the radiochemical work for the thermal fission of U^{235}. The observed increase in the charge density with the fragment mass in the region of mass 90-106 is not understood on the basis of any proposed hypothesis.

Table I. Tentative Assignment of Prompt Gamma-Ray Lines.

Z±1	A±1	E_γ(keV)	$T_{\frac{1}{2}}(10^{-9}$ sec)	K Electron Located
43	106	170	>0.5	Yes
44	108	123	<0.5	Yes
44	109	419	<0.5	Yes
44	110	572	<0.5	Yes
		508	<0.5	Yes
		239	<0.5	Yes
		149	>0.5	Yes
		98	0.8±0.2	No
		76	>0.5	No
44	112	210	<0.5	Yes
		158	<0.5	Yes
		103	0.5±0.2	No
46	116	125	<0.5	No
47	116	145	<0.5	No
54	138	420	<0.5	Yes
54	139	586	<0.5	Yes
		582	<0.5	Yes
		568	<0.5	Yes
		382	<0.5	Yes
54	140	479	<0.5	Yes
		453	<0.5	Yes
54	142	488	<0.5	Yes
55	139	394	<0.5	Yes
55	140	371	<0.5	Yes
		365	<0.5	Yes
56	144	354	<0.5	Yes
		111	0.6±0.2	No
60	150	261	<0.5	No
		134	——	Yes
59	150	245	<0.5	No
		120	<0.5	Yes

REFERENCES AND FOOTNOTES

* On leave of absence from the Atomic Energy Establishment, Trombay, Bombay, India.

[1] BOWMAN, H. R. and THOMPSON, S. G., in Proceedings of the Second International Conference on the Peaceful Uses of Atomic Energy, Geneva (1958) 212-216, Paper P/652.

[2] BOWMAN, H. R., THOMPSON, S. G., MILTON, J. C. D., and SWIATECKI, W. J., Phys. Rev. 126 (1962) 2120.

[3] BOWMAN, H. R., THOMPSON, S. G., MILTON, J. C. D., and SWIATECKI, W. J., Phys. Rev. 129 (1963) 2133.

[4] THOMPSON, S. G., STREET, K., GHIORSO, A., and SEABORG, G. T., Phys. Rev. 80 (1950) 790.

[5] NAKAMURA, M., and LA PIERRE, R., Lawrence Radiation Laboratory Report UCRL-11494, June 1964.

[6] FRASER, J. S., MILTON, J. C. D., BOWMAN, H. R., and THOMPSON, S. G., Can. J. Phys. 41 (1963) 2080.

[7] MALMFORS, K. G., Arkiv Fysik, Band 13, No. 21 (1957).

[8] WAPSTRA, A. H., NIJGH, G. J., VAN LIESHOUT, R., Nuclear Spectroscopy Tables, North-Holland Publishing Co., Amsterdam (1959).

[9] ANDREEV, D. S., GRINBERG, A. P., GUSINSKII, G. M., EROKHINA, E. I., and LEMBERG, I. Kh., Izvestia Akad. Nauk USSR (Ser. Phys.) 24 (1960) 1474.

[10] MILTON, J. C. D., Lawrence Radiation Laboratory Report UCRL-9883 Rev. (1962).

[11] PAPPAS, A. C., Proceedings of the International Conference on the Peaceful Uses of Atomic Energy, VII, United Nations, Geneva (1955) 19-26.

[12] GLENDENIN, L. E., GRIFFIN, H. C., and UNIK, J. P., (private communication).

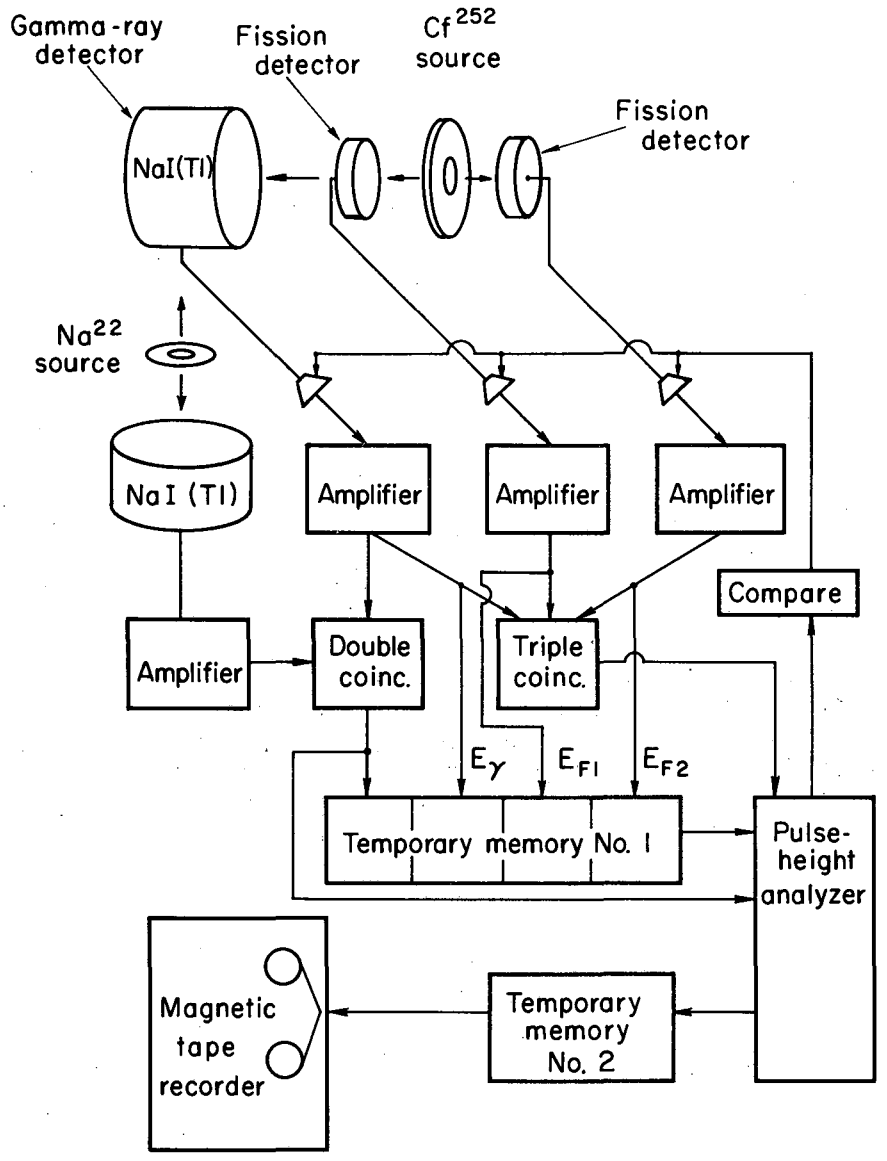

Fig. 1. Schematic diagram of the experimental arrangement used in these experiments. The NaI detector was used in the early gamma-ray measurements and was later replaced with a lithium-drifted germanium detector for high resolution gamma-ray measurements and a lithium-drifted silicon detector for measuring the electron and the X-ray spectra.

Fig. 2. (a) Total prompt gamma-ray energy distribution from the spontaneous fission of Cf^{252} (using a NaI detector).

(b) Spectra of prompt gamma rays associated with various values of mass ratio (M_H/M_L).

(c) The dependence of prompt gamma-ray energy on the velocity and direction of motion of the fragments. The dashed and solid lines represent the gamma-ray spectra for the two cases: (1) when the heavy fragments (M=140±2) were moving towards the gamma-ray detector and (2) away from the detector.

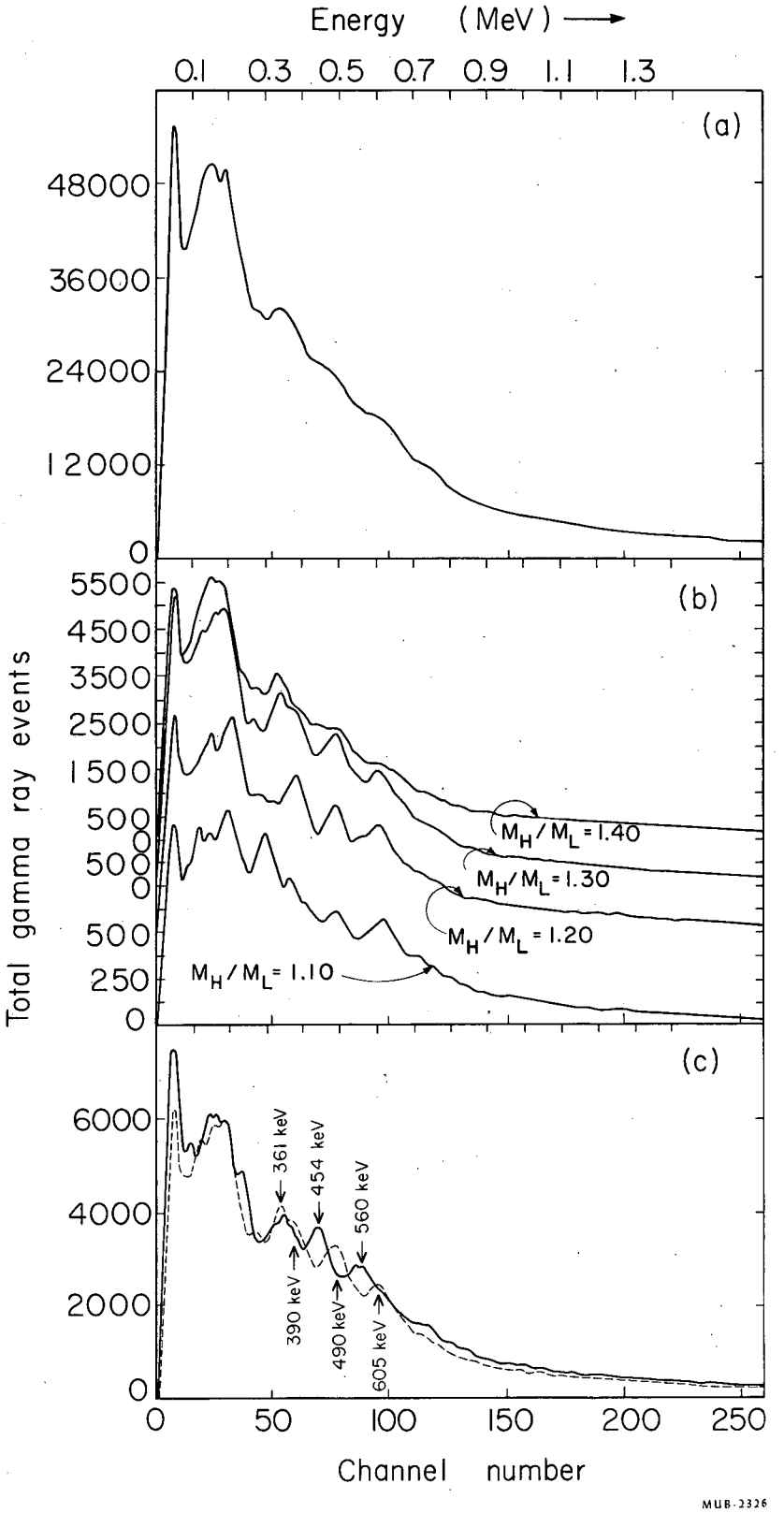
Energy (MeV) →
0.1 0.3 0.5 0.7 0.9 1.1 1.3
(a)
48000
36000
24000
12000
0
(b)
5500
4500
3500
2500
1500
500
0
500
0
500
250
0
M_H/M_L = 1.40
M_H/M_L = 1.30
M_H/M_L = 1.20
M_H/M_L = 1.10
(c)
6000
4000
2000
0
361 keV
454 keV
560 keV
390 keV
490 keV
605 keV
0 50 100 150 200 250
Channel number
Total gamma ray events
MUB-2326

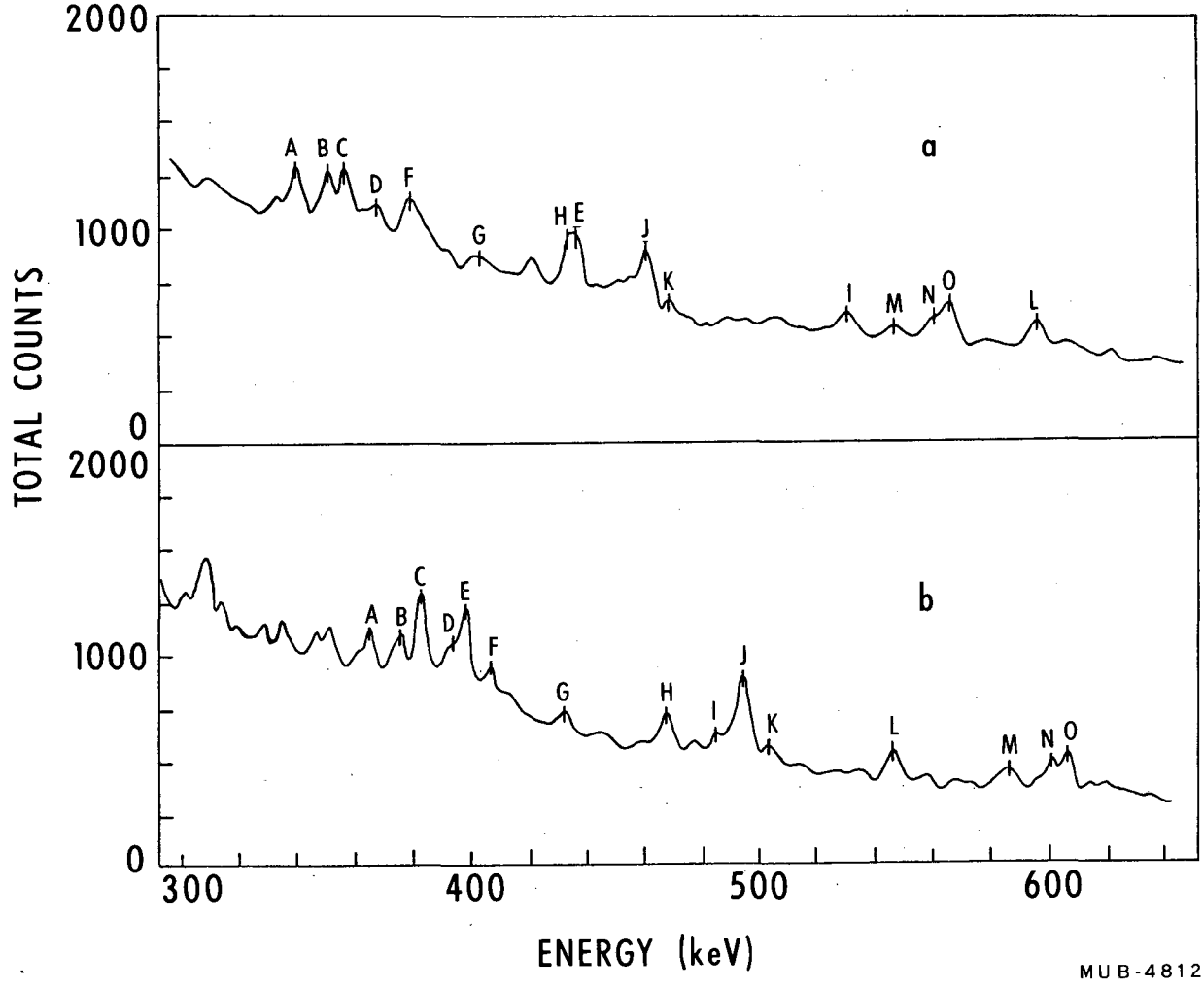

Fig. 3. The prompt gamma-ray spectra measured with a lithium-drifted germanium detector for the fragment mass ranges of 109-111 (137-139): (a) light fragments moving towards the gamma-ray detector and (b) heavy fragments moving towards the gamma-ray detector.

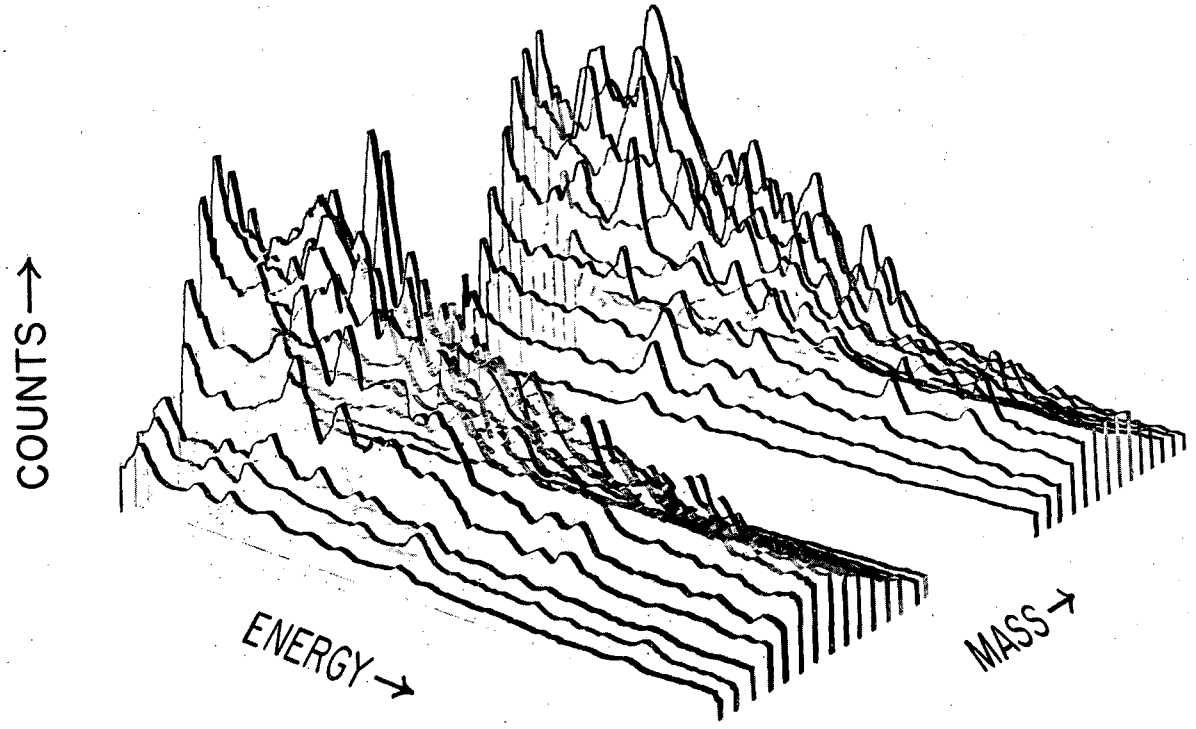

Fig. 4. The observed prompt gamma-ray energy spectra below 300 keV for selected intervals of fragment mass.

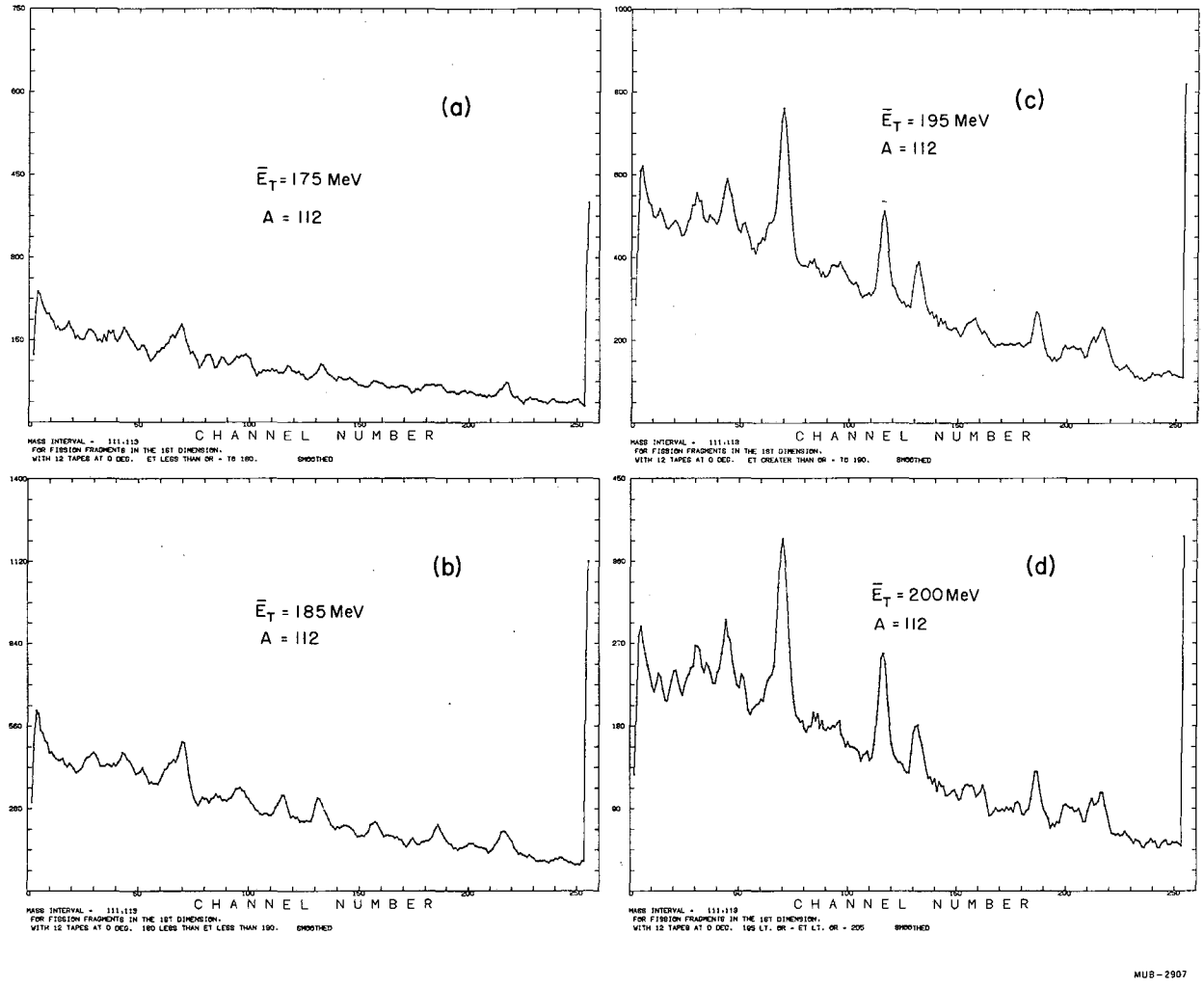

Fig. 5. The prompt gamma-ray energy spectra (below 300 keV) sorted according to total kinetic energy (E_T) for a single interval of fragment mass.

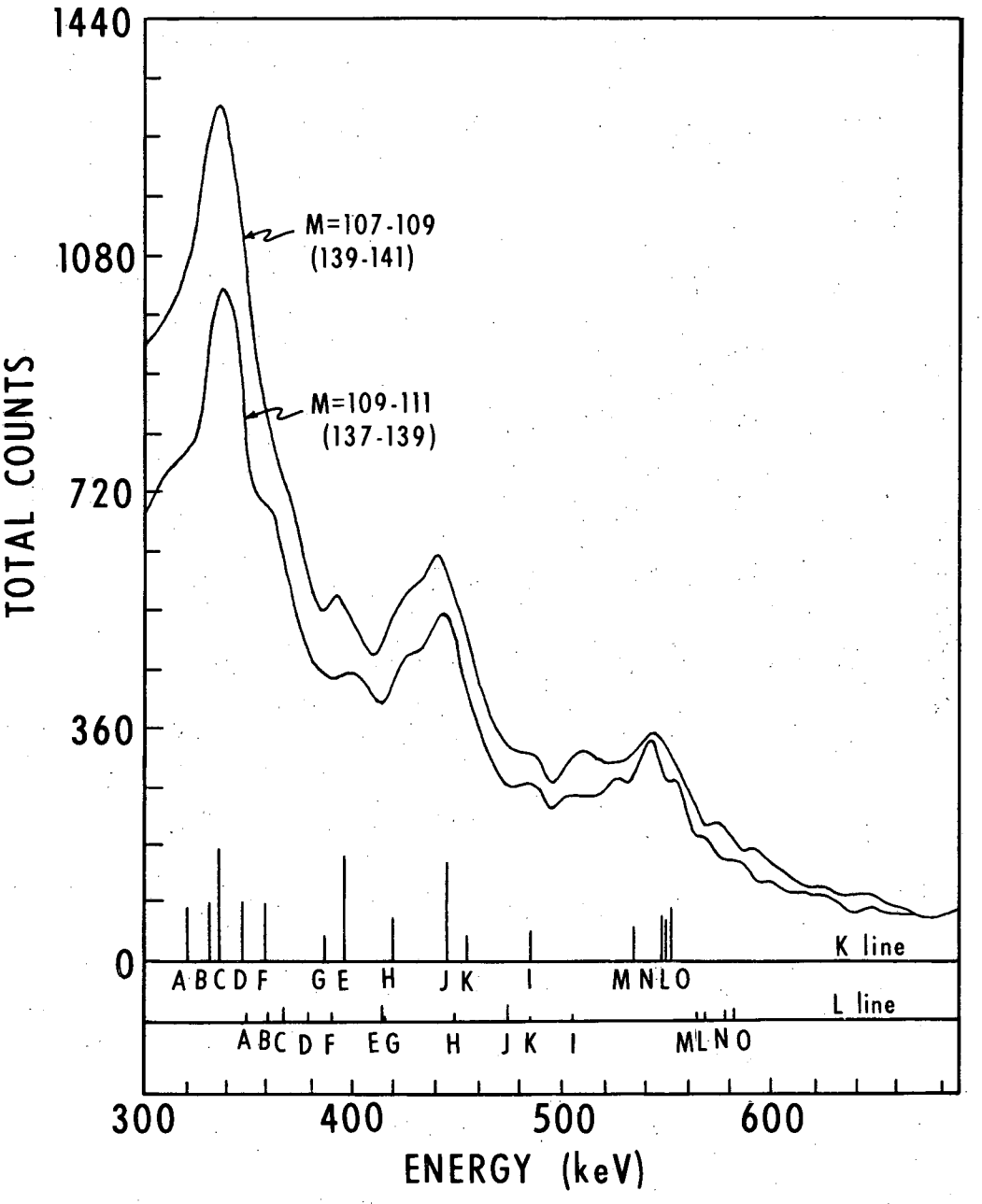

Fig. 6. The prompt electron energy spectra associated with fission fragment mass (a) 107-109 (139-141) and (b) 109-111 (137-139). The vertical lines at the bottom are the calculated locations of K and L-electron lines using gamma-ray data from Fig. 3. As a rough guide, the line lengths are taken from the intensities of the gamma rays.

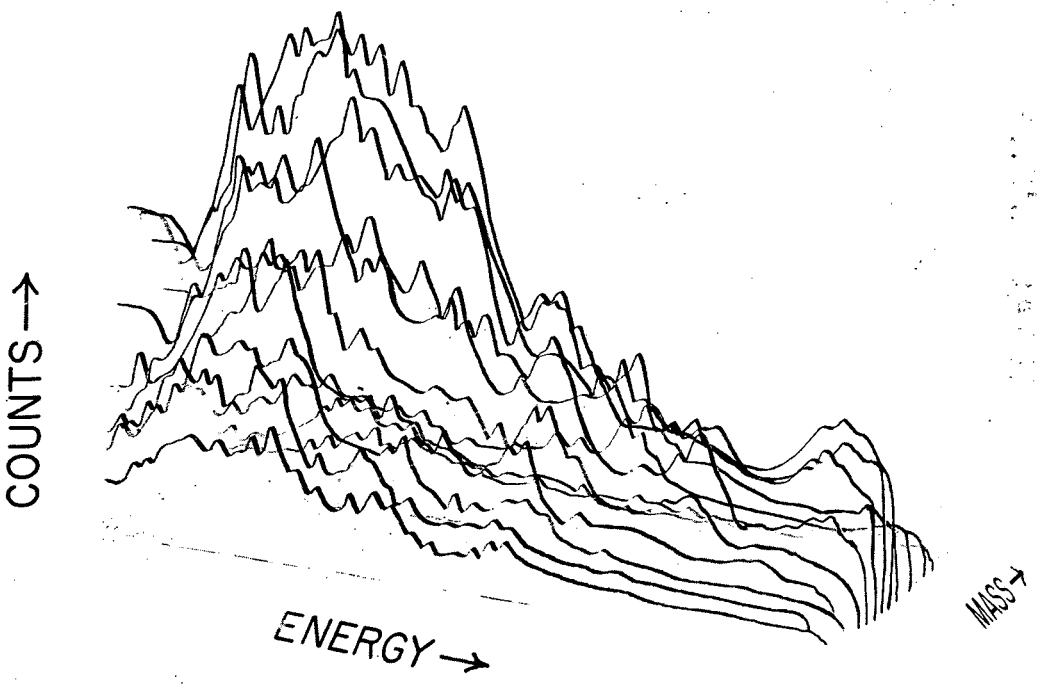

Fig. 7. The prompt electron energy spectra (below 300 keV) for selected intervals of light fragment mass. Electron spectra measured at 90° to the direction of motion of the fragments are identical for light and heavy fragment pairs.

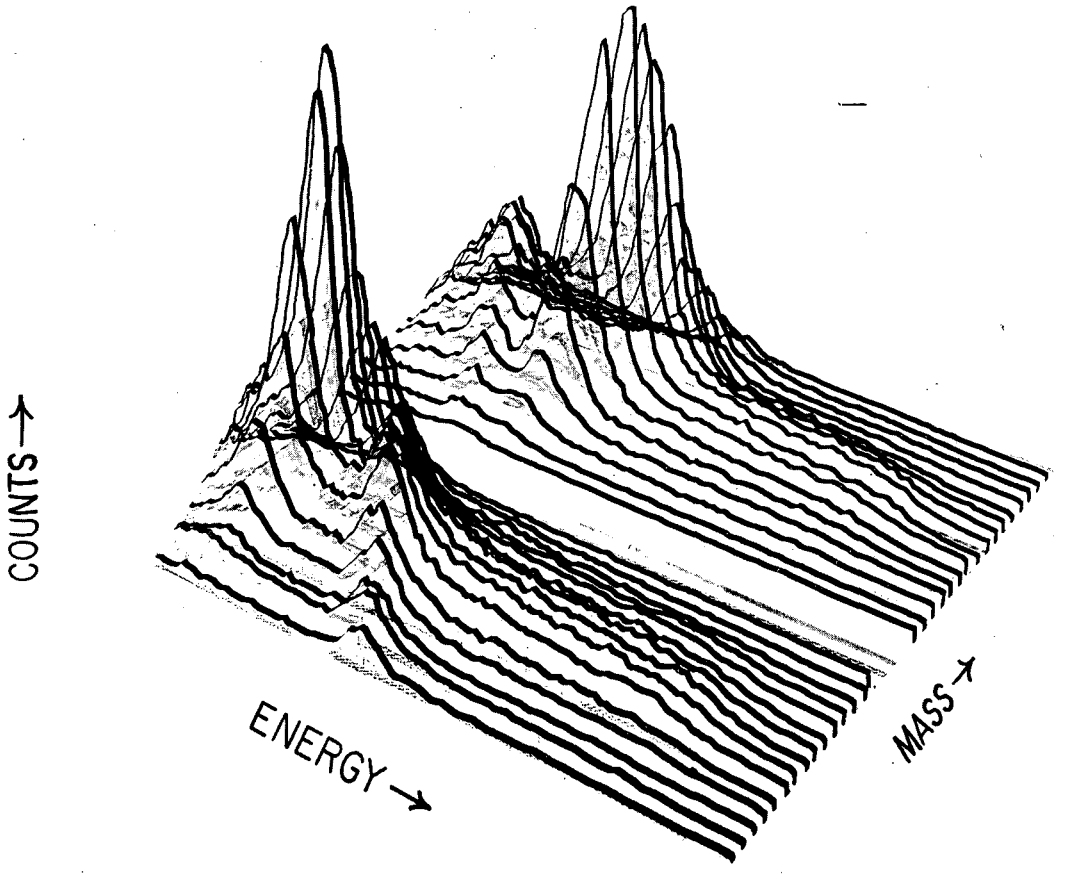

ZN-4602

Fig. 8. The observed energy spectra of prompt K X-rays for 36 intervals of the fragment masses moving towards the detector.

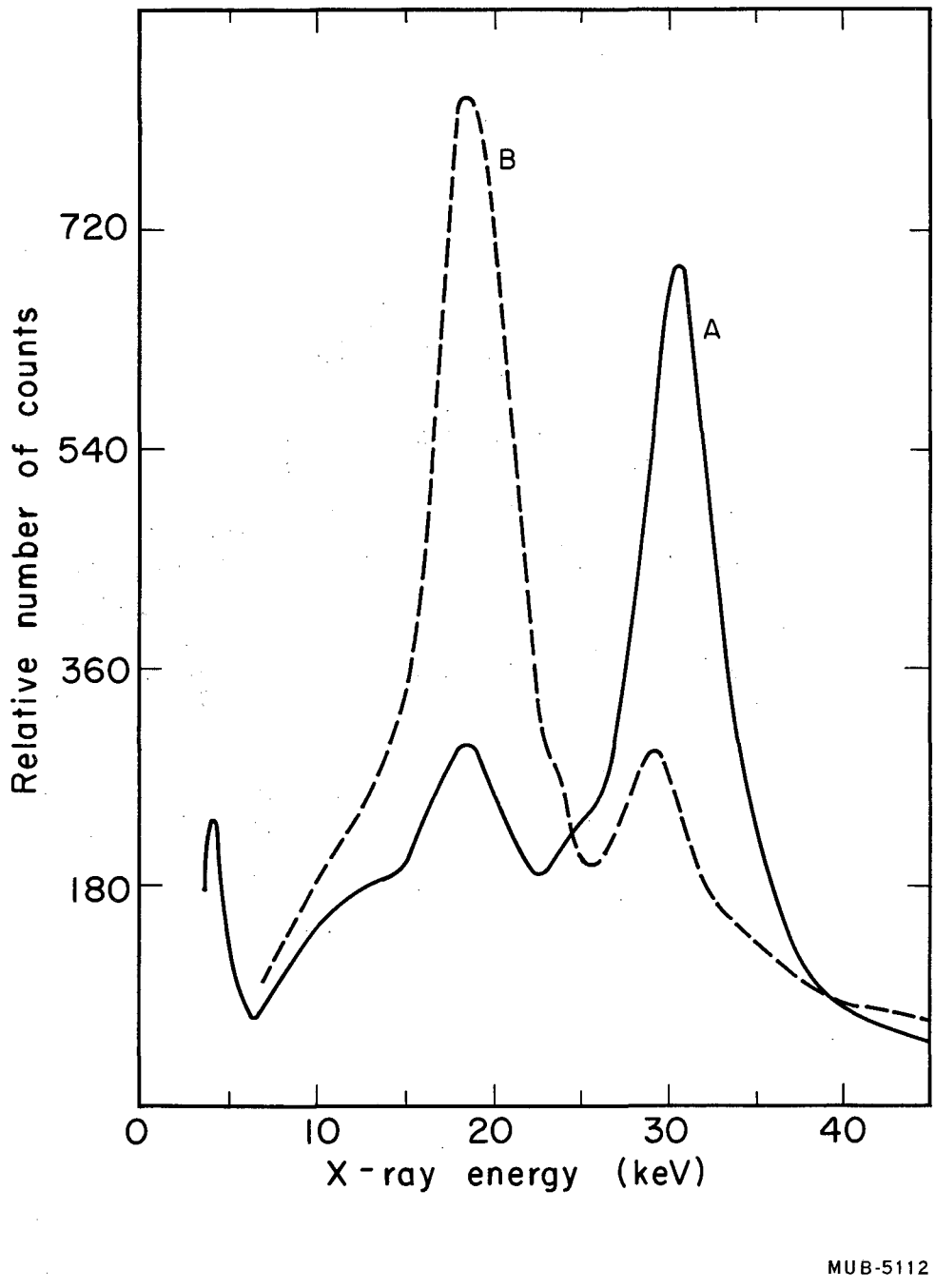

Fig. 9. The measured prompt K X-ray energy spectra in coincidence with mass 140 moving (a) toward and (b) away from the X-ray detector.

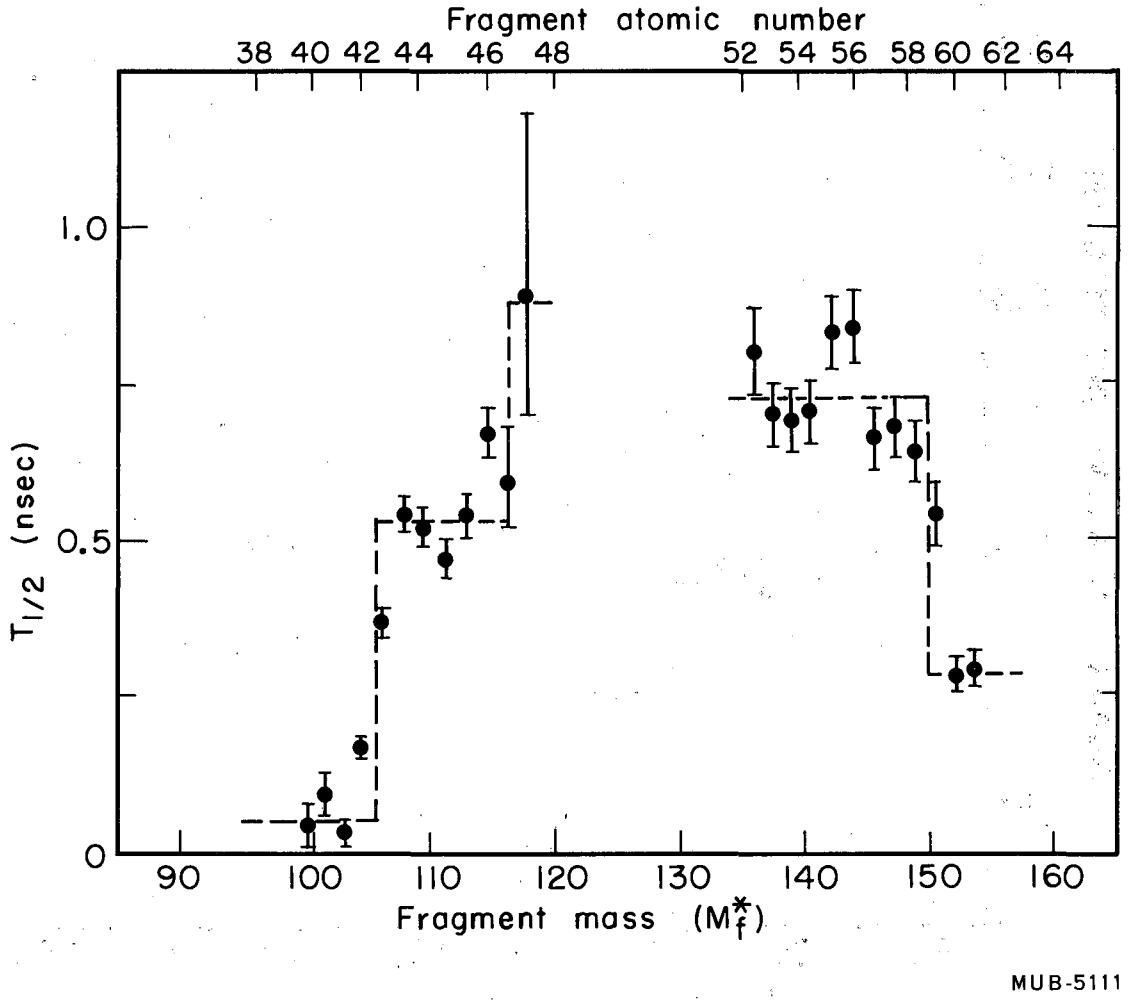

Fig. 10. The measured half life for K X-ray emission as a function of the final masses (M_f^*) and atomic numbers of the fission fragments (corrected for mass dispersion).

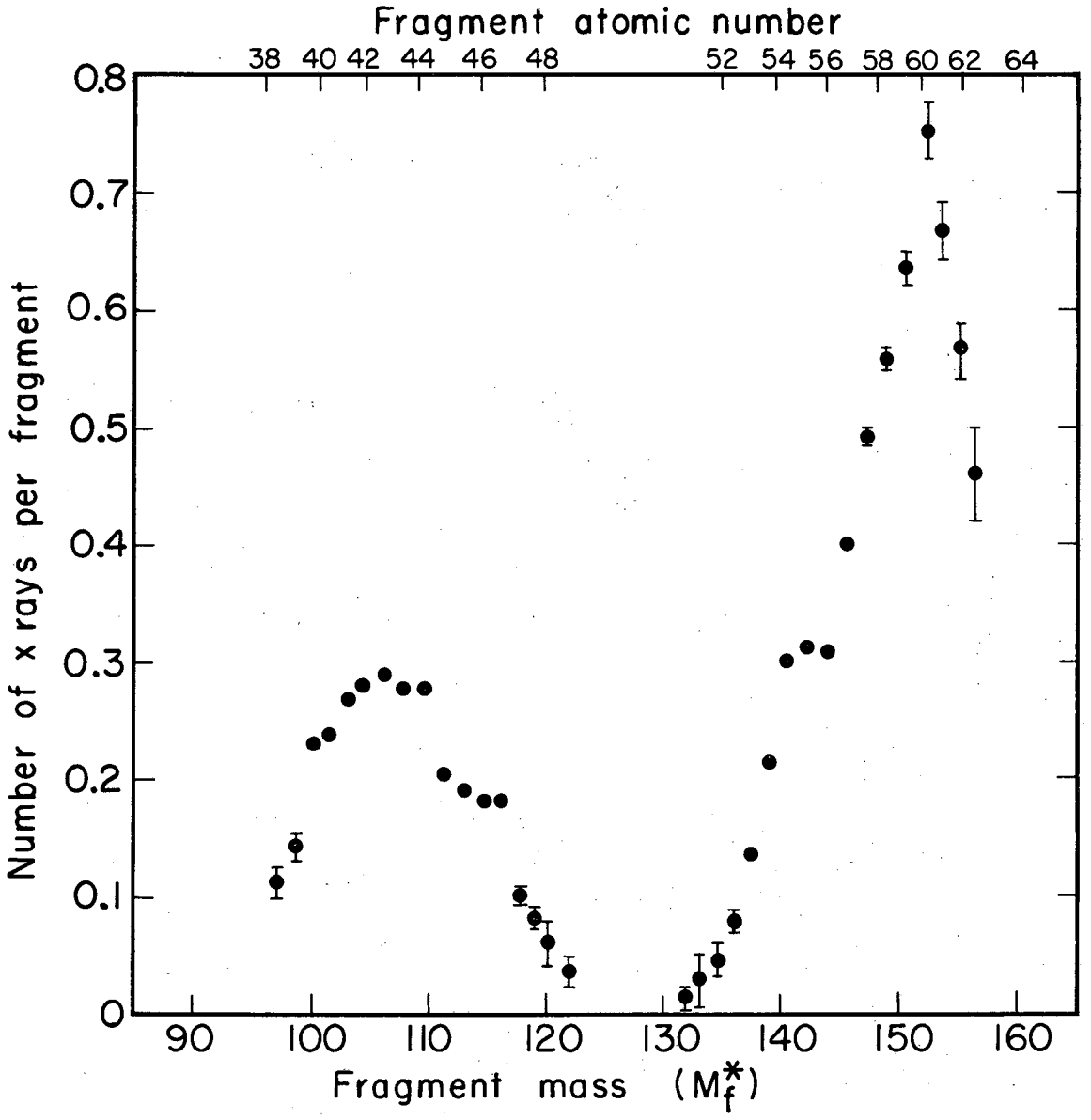

Fig. 11. The observed yield per fragment of K X-rays as a function of final masses (M_f^*) and atomic numbers of the fission fragments (corrected for mass dispersion).

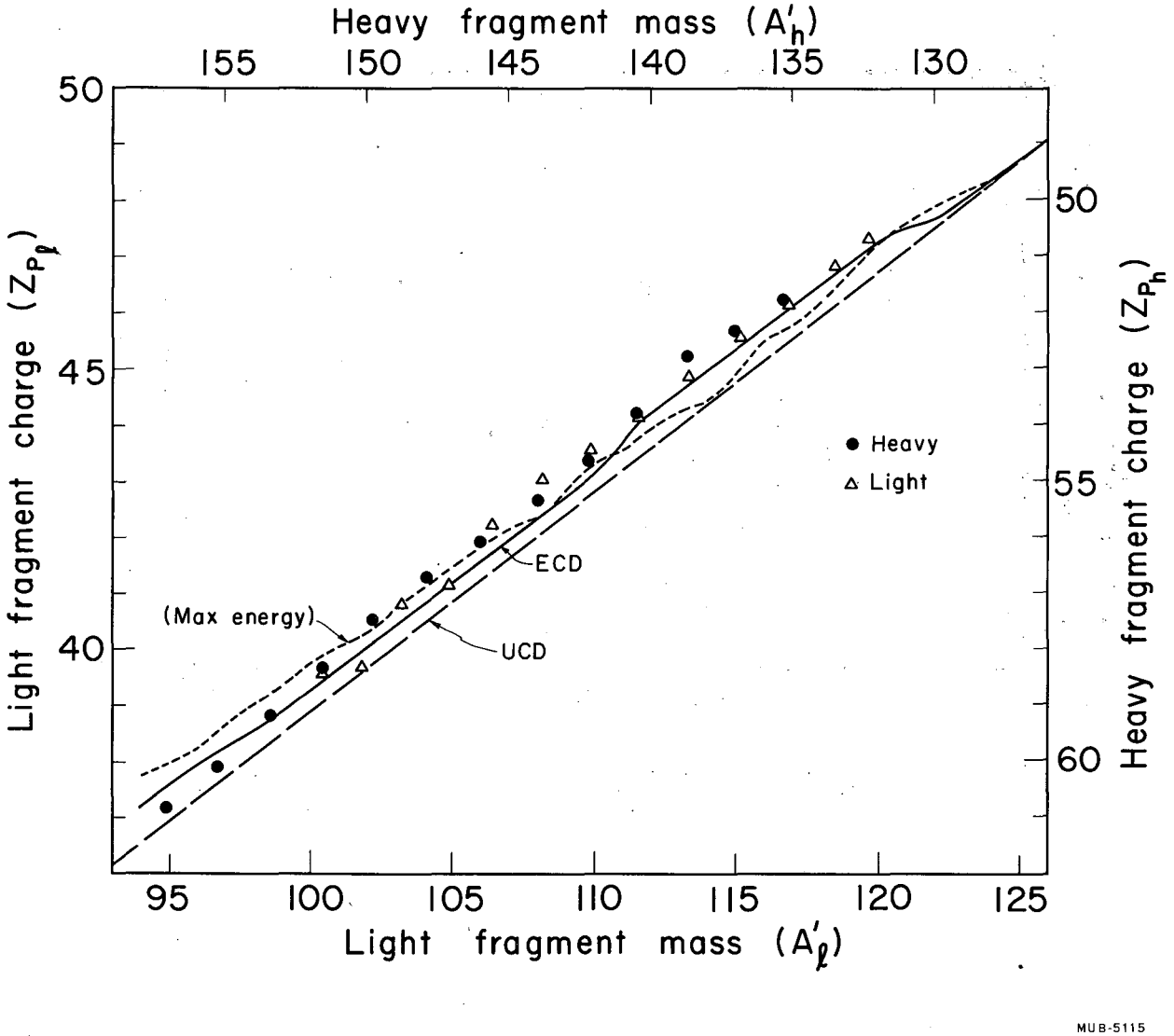

Fig. 12. The most probable charge (Z_p) versus the initial mass of the fragments (A_i) (corrected for mass dispersion) as determined from the X-ray measurements. The curves calculated on the hypothesis of maximum energy released, equal charge displacement (ECD) and unchanged charge distribution (UCD) are also shown in the figure.

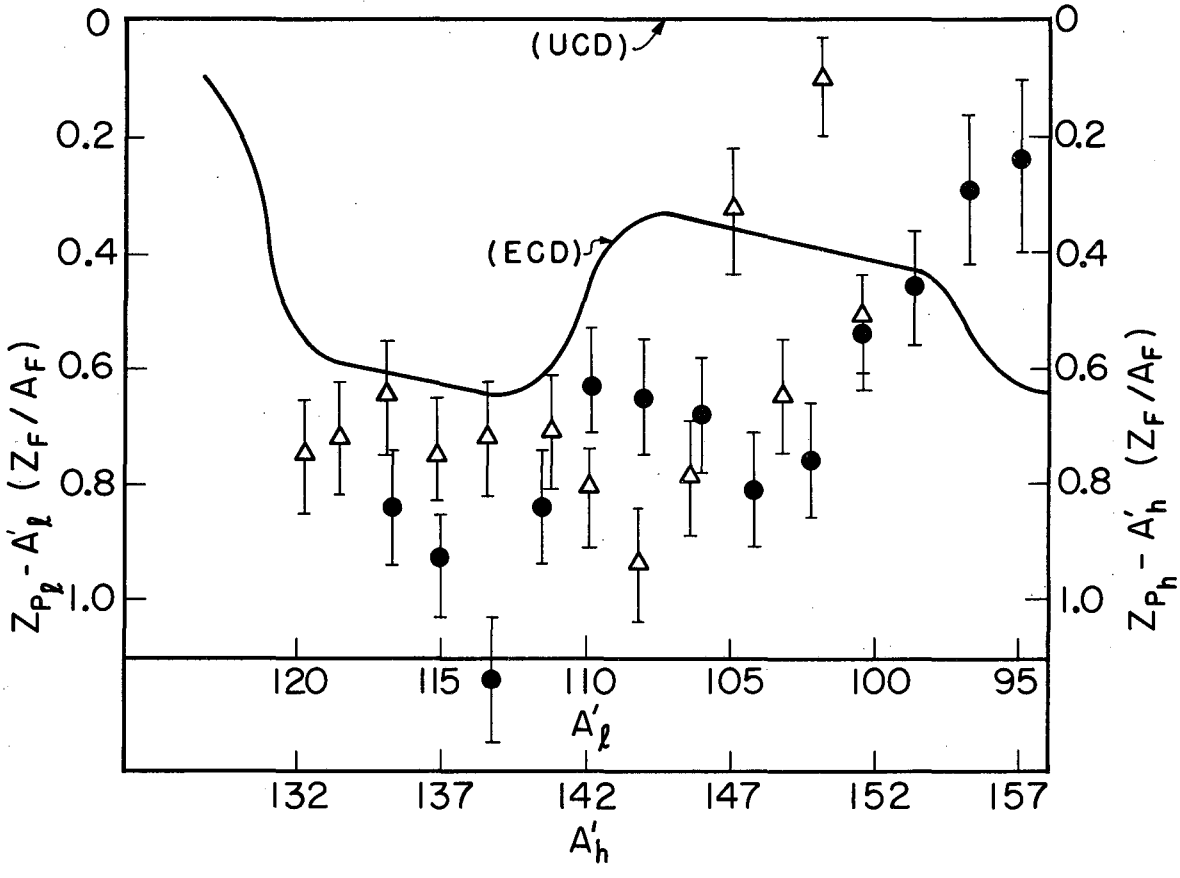

Fig. 13. The deviation of the measured charges from the unchanged specific charge, plotted on a complimentary scale for the light and heavy fragments.